05

Experimental study of the superconducting RFTES detector with bridge inductively coupled to a resonator

© N.Yu. Rudenko,[1] V.I. Chichkov,[1] S.V. Shitov[1,2]

[1]National University of Science and Technology MISiS,
119049 Moscow, Russia
[2]Kotelnikov Institute of Radio Engineering and Electronics, Russian Academy of Sciences,
125009 Moscow, Russia
e-mail: ny.rud@yandex.ru, sergey3e@gmail.com

Received May 15, 2025
Revised May 15, 2025
Accepted May 15, 2025

The development and experimental study of the superconducting detector based on RFTES technology with inductive coupling of the thermistor microbridge made of hafnium in a quarter-wave resonator is described. An analysis of a model of the superconducting differential detector of the terahertz range, consisting of two RFTES detectors with different types of coupling in a quarter-wave resonator, providing a balance of losses in the resonator with simultaneous irradiation of both antennas, is carried out. The manufacturing technique and comparison of the calculated *S*-parameters with preliminary results of microwave measurements of the RFTES detector at a temperature of about 130 mK are presented. For warming up the RFTES detector with the carrier signal power, the following were obtained: maximum amplitude conversion slope $9 \cdot 10^8\ \mathrm{W}^{-1}$ and maximum frequency (phase) conversion slope during inductive frequency transition $3.2 \cdot 10^{13}$ Hz/W.

Keywords: RFTES bolometer, high-Q resonator, differential detection, thin-film bridge, hafnium.

DOI: 10.61011/TP.2025.09.61844.121-25

Introduction

Detectors based on the RFTES (Radio Frequency Transition Edge Sensor) technology can be used to study cosmic rays in the terahertz range of the electromagnetic spectrum [1,2], for use in quantum nanosystems [3] and security systems [4]. The principle of operation of the RFTES detector is the linear transformation of the thermal power of the input signal, P_{in}, absorbed in a superconducting thin-film bridge, into a variation of the microwave carrier power at the resonator frequency, ΔP_{out}. Such a conversion is possible with an amplification, formally defined as $G = \Delta P_{out}/P_{in}$; in this case, a quadratic power conversion occurs at the terminal detector, which makes it possible to control the RFTES detector and to canalize the reading signal using the 50 Ω standard (via coaxial cables). The significant power gain observed in the experiments makes it possible to reduce the noise requirements for the buffer cooled amplifier. The possibility of integrating a superconducting amplifier into the resonator of such a detector motivates the development of a more complex device — active superconducting detector [5].

The detector response occurs due to a change in the impedance of the thermoresistive element of the thin-film bridge near the superconducting transition at a frequency of 1.5 GHz, which is caused by the release of heat when the bridge absorbs terahertz photons and photons at the carrier frequency. Such a change in the impedance of the absorber included in the resonator leads to a modulation of the transmission coefficient of the resonator excitation line. The power transfer coefficient of the carrier from the excitation line to the detector absorber determines the preheating in the operating mode, its value depends both on the parameters of the bridge itself and on the embedding impedance of the resonator. A distributed resonator in the form of a quarter-wave segment of a waveguide can be roughly divided into two parts: an inductive part located near the closed end of the waveguide, and a capacitive part near the open end. These parts are characterized by a large current in the inductive part (stores magnetic energy) and a large field in the capacitive part (stores electrical energy), which is similar to a lumped oscillatory *LC*-circuit. Shifting the insertion point of the detector along the resonator allows the bridge to be matched over a wide range of resistances, as described in Ref. [6].

The signal heating is created by terahertz photons coming from the planar antenna. The microwave reading current (carrier current) at the resonator frequency works as an additional heater, which is set higher the lower the substrate temperature relative to the temperature of the superconducting transition. An increase in microwave heating power leads to an increase in the conversion coefficient (gain) according to model calculations and experimental studies [2]. A superconducting bridge with an electron gas near a critical temperature is capable of detecting radiation in a very wide frequency band from the order of 1 to 1000 GHz. It was shown in Ref. [7] that in the RFTES detector there is practically no dependence of the sensitivity of the transmission coefficient S_{21} on the

frequency of the heating current of the absorber bridge. This property of the RFTES absorber allows to conclude that if the thermal power supplied to the bridge from microwave reading/pumping at a frequency of 1.5 GHz and the radiation power of the bridge with a terahertz blackbody signal in the band of 550–750 GHz remain constant in total, then even with a change in the ratio between these contributions, the resonant dip S_{21} remains unchanged. This is of great methodological importance, since it allows us to determine the coefficients of power transmission to the bridge from various sources, including the absorption coefficient of a thermodynamic noise source (blackbody) with accuracy up to the reception band of a terahertz antenna, which can be calculated fairly accurately using classical electrodynamics.

One of the main features of the reading of the RFTES detector, in comparison with the MKID (Microwave Kinetic Induction Detector), is the invasive heating of the electron gas (quasi-particles) in the volume of the bridge, necessary to heat the absorber to the optimal temperature, T_0, inside the narrow temperature range of the superconducting transition. Due to the fact that the pairing energy tends to zero near the temperature of the superconducting transition, the recombination noise in the RFTES detector is low, and there is no need to use ultra-weak reading signals in an attempt to reduce recombination noise, which is typical for MKID detectors.

Due to this specificity of the RFTES detector in the temperature range of 200–400 mK, its own noise can be significantly lower than corresponding MKID noise, which is discussed in Ref. [8]. This circumstance makes it possible to consider the RFTES detector as a candidate for promising space missions using a sorption refrigerator capable of operating in zero gravity.

Previously, prototypes of RFTES detectors [2] were created and tested, which demonstrated the sensitivity of $\sim 10^{-17}\,\mathrm{W}/\sqrt{Hz}$, which confirmed the feasibility of further development of the approach [9] . A theoretical consideration of the coupling scheme of a nonlinear bridge absorber with a resonator [10,11] led to the understanding that shifting the insertion point of the antenna with the bridge to the inductive part of the oscillatory circuit (to the closed end of the quarter-wave resonator, which is similar to MKID [12]), allows changing the sign of the detector response to the opposite. Combining two detectors with opposite response signs on a single chip into one common resonator makes it possible to implement the principle of differential signal reception, which is similar to the operation of a differential amplifier. The differential detector contains one quarter-wave resonator and two antennas with absorbers. These two sensors are conventionally called *C*-type and *L*-type detectors. They differ in the way the bridge is connected to the resonator. The chip on which the two detectors are placed integrates with the immersion lens on its flat surface so that the planar antennas are located in the focal plane of the lens at a distance corresponding to the diffraction resolution of the optical system, i.e., the antenna diagrams close without a significant gap between them (the intersection level is about −10 dB). The distance between the antennas should be about 200 μm to ensure small spherical aberrations of the system according to calculations in Ref. [13], and they should be located symmetrically relative to the optical axis of the lens. The advantage of the differential response is to suppress atmospheric fluctuations and increase the contrast of the boundary of an extended object. The principle of the differential detector was developed and applied to optimize the matching circuit in the active-superconducting detector (ASD) [5]. To do this, the *DC*-SQUID is included in the inductive resonator circuit instead of the *L*-detector, as described in Ref. [14].

The developed circuit of *L*-connection of the antenna with a bridge to a resonator circuit, according to the authors, will allow experimentally testing the concept of inductive switching and it will later facilitate the resolution of the task of connecting a SQUID to a resonator using known circuit parameters. The purpose of this work is to experimentally confirm the operability of the new RFTES detector of *L*-type and to outline a further path for studying the differential structure.

1. Analysis of schemes for the coupling of a bolometric bridge in a resonator

The principle of partial inclusion consists in the fact that only a small portion of the resonator current passes through the nonlinear resistive element. The application of this principle makes it possible to calculate the optimal coupling parameters for any preset impedance so that the Q-factor of such a resonator meets the specified requirements. The circuits shown in Fig. 1, *a, b* correspond to two cases of a resonator with a nonlinear resistive absorber (thermistor), for which the active component of the impedance is reduced:

1) using a small serial capacitor;

2) when using a low-inductive shunt.

Fig. 1, *a* shows a scheme of a band-stop filter that limits the current of the pass-through line; Fig. 1, *b* shows a filter circuit that limits the voltage in the pass-through line. Both filters limit the transmission coefficient of the transmission line at the resonant frequency due to reflection and partial (no more than 50 %) absorption. The heating of the thermistor by the signal power absorbed by it correlates with a change in the depth of the dip (degree of suppression), $\min(|S_{21}|^2)$, at the resonant frequency. The response refers to a change in the depth of the dip $\Delta|S_{21}|^2$ depending on the heating of the bridge from the superconducting state to the value „*Bridge resistance*“ (Fig. 1, *c, d*).

In the case of the *C*-detector, a nonlinear resistive bridge is connected to the resonator circuit using a capacitive divider $C_x/C_R \sim 0.01$ (Fig. 2, *a*), thus limiting the current through the resistive element and losses in the resonator. At the same time, the resonator frequency does not change,

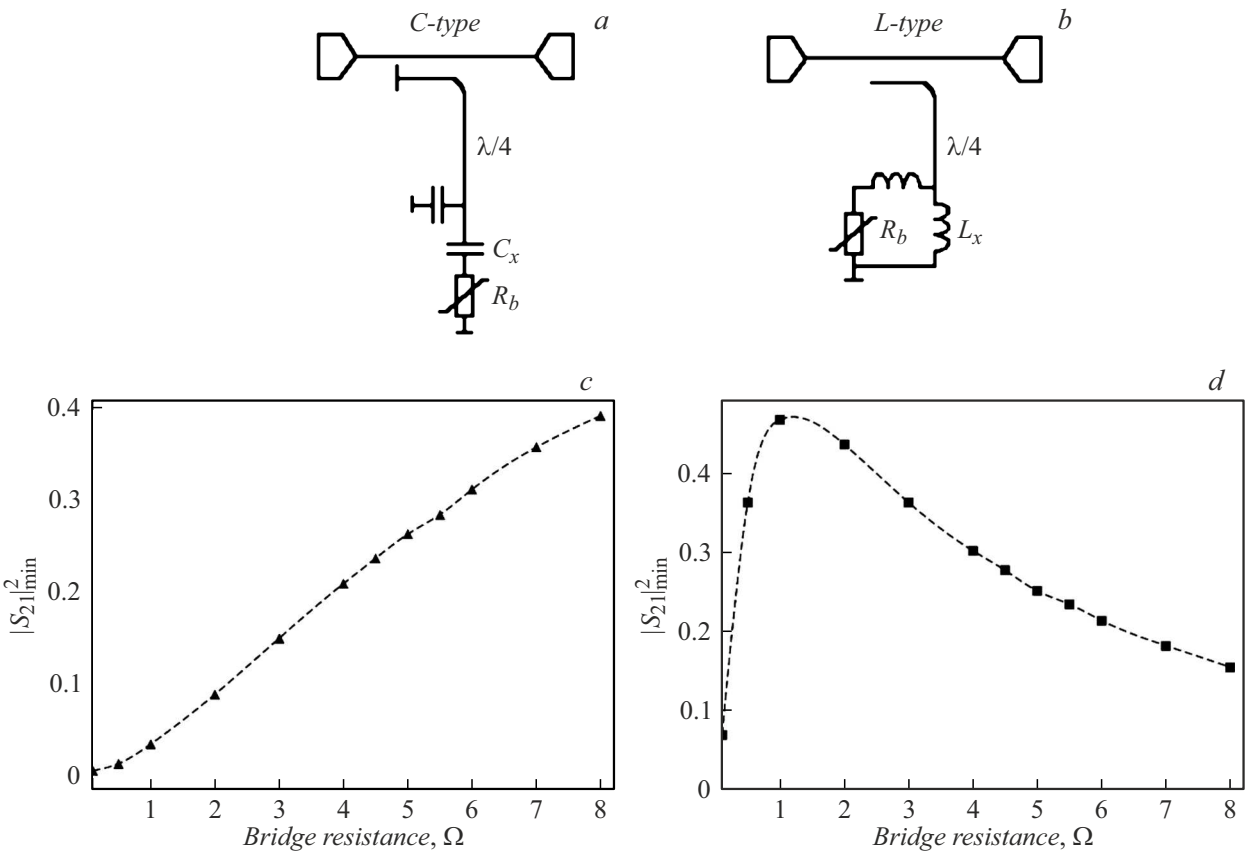

Figure 1. Conceptual schemes (a) and (b) and detector response (c) and (d) for two ways of including a relatively high-resistance bridge in a quarter-wave resonator while maintaining high Q-factor of the system $Q \approx 10^4$. Here and below it is assumed that each nonlinear element is connected to a planar antenna, which supplies it with a heating current at terahertz frequency (antennas are not shown in the diagrams, they are considered as virtual heat sources). Circuit a — connection of C-type in the region of the capacitive impedance of the resonator; circuit b — connection of L-type in the inductive region of the resonator. Calculated dependences of the transmission coefficient of the transmission line (a) and (b) on the resistance of the nonlinear resistive bridge: c — the value of the minimum transmission of $|S_{21}|^2_{\min}$ at the carrier frequency of the resonator as a function of the resistance of the bridge in the RFTES detector with C-type connection; d — for a detector with L-type connection.

since the capacitive nature of the impedance in the circuit of the nonlinear element is maintained for all values R_b. When using an inductive shunt, the process of the circuit evolution turns out to be more complicated. The response in the form of an increase in transmission dominates (response of C-type) in case of a transition of nonlinear element from a negligibly small value of R_b to values comparable to the parasitic impedance of the circuit in series to an inductive shunt. In the region of comparable values of the resistive impedance of the bridge and the impedance of the parasitic inductance, the nature of the current changes dramatically from inductive at low values of R_b, when the phase is determined by the parasitic inductor L_{x2} (≈ 100 pH), to resistive when the impedance of the nonlinear absorber becomes dominant (Fig. 2, b). This can be described qualitatively as a smooth uncoupling of the parasitic inductor in the bridge circuit along with an increase of R_b, which leads to a change in the resonant frequency of the system $F_0 = 1/2\pi\sqrt{L_R C_R}$ ($L_R = 3.8$ nH, $C_R = 2.8$ pF). The current through the bridge is determined by the impedance of the shunt $L_{x1} \approx 5$ pH in case of further heating, after overcoming the value of $R_b \approx 1\,\Omega$.

For the coupling element of the resonator in Fig. 2, c with the excitation/reading line, a symmetrical circuit has been selected, which is applicable in both the case of capacitive and inductive coupling, containing an inductive coupling L_m and equivalent capacitances C_{c1} and C_{c2}, which are attributes of any distributed line. For inductive coupling with a Q factor of $Q \sim 5 \cdot 10^4$ in a L-type detector in Fig. 2, b, the lumped elements have a value of $L_m \approx 0.22$ nH with a magnetic coupling coefficient between the inductors $K_{12} = 0.025$ and $C_{c1} \approx 13$ fF.

In a properly tuned differential detector, the change in the Q-factor of the resonator during synchronous heating of the two bridges should be negligible. The selection of circuit parameters consists in fulfilling the condition of equality of losses r_b introduced by each bridge connected to the corresponding end of the quarter-wave resonator, which meets the condition $r_b \approx (\omega L_{x1})^2/R_b = R_b(C_x/C_R)^2$, pro-

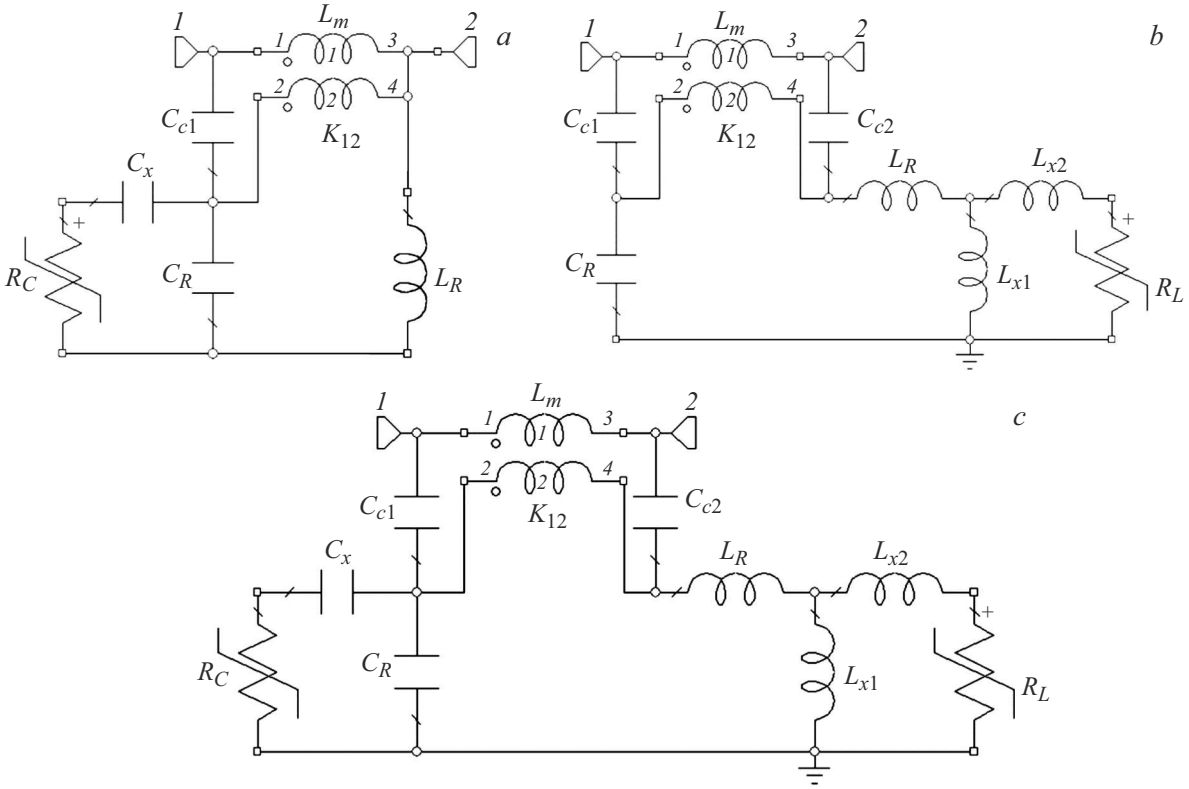

Figure 2. Conceptual (equivalent) schemes of the RFTES detector family: *a* — for a detector with connection of *C*-type; *b* — for a detector of *L*-type with indication of the majority parasitic elements; *c* — for a differential detector. The antennas are not shown in the diagram, and it is assumed that the signal is supplied as heat to the nonlinear elements R_C and R_L.

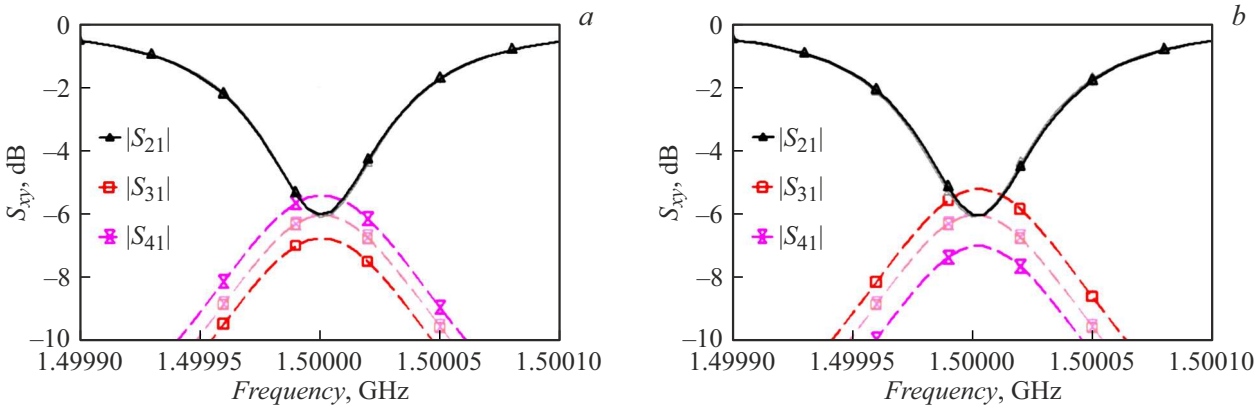

Figure 3. Response of the electromagnetic model of the differential detector to the same terahertz signal absorbed by both bridges. The graphs show that the transmission S_{21} does not change (the gray and black curves are barely distinguishable, triangles), as the increment of the power absorption coefficient S_{31} and S_{41} in the bridges at the ports *3* and *4* (Fig. 2, *c*) are the same in modulus, but have the opposite sign (the squares and bows are reversed).

vided that $L_R \gg L_{x1}$ and $C_R \gg C_x$. The above relationship corresponds to the complete matching of the two bridges with the external circuit (with the resonator). The total losses $2r_b$ in the resonator (Fig. 2, *c*) have different signs of the temperature loss coefficients depending on which of the two bridges heats up more strongly. With the same heating ($R_C = R_L$), there is no change in the depth of the dip S_{21}, as shown in Fig. 3.

The heating of the two bridges ceases to be the same only when there is a non-zero difference in the intensity of the terahertz radiation incident on each of the detectors. Only under this condition does the transmission level in the reading line increase or decrease. In this case, the increment sign indicates the direction of the incident radiation gradient. The principle of differential reading can be applied to calibrate the circuit for insertion of a parametric microwave

amplifier based on a *DC*-SQUID into a resonator with *C*-detector [13]. The unknown input impedance of the SQUID can be found by comparing it with the impedance of the bridge in the *L*-detector: the effect of the SQUID on the Q-factor of the resonator in the matched mode should be the same as that of the *L*-bridge. In summary, the use of the *L*-detector is an important step towards implementing differential signal reading and creating an active superconducting detector.

2. Experimental results and discussion

The full development cycle of the real electromagnetic structure of the *L*-detector includes several stages:

1) finding optimal element parameters in the limit of a lumped circuit (Fig. 2, *b*);

2) creation of an electromagnetic model of a terahertz antenna with a bridge integrated into a resonator circuit at a frequency of about 1.5 GHz, including a coupling element with a reading/excitation line according to Fig. 1, *b*;

3) estimation, based on experimental data, of the detector conversion coefficient;

4) solving the problem of finding the temperature dependence of the $R_b(T)$ bridge based on experimental data on the temperature dependence of the transmission $\min(S_{21}(T))$. Stage 4 has mainly an academic focus; it allows us to assess how closely the nonlinear impedance obtained in the experiment corresponds to the hypothesis of the applicability of the Mattis-Bardeen theory to a thin hafnium film, which is currently the main nonlinear element of the RFTES detector.

The electromagnetic circuit was calculated in the AWRDE simulation environment using the EMSight calculation core, which uses the method of moments and has proven its effectiveness in the case of planar superconducting structures [15]. The boundary conditions were set by a conductive box with an open upper and lower boundary; the planar 3*D* structure consisted of a metallization layer (an ideal conductor) and three dielectric layers simulating: a silicon substrate with a dielectric constant $\varepsilon = 11.7$ and a thickness of $t = 500\,\mu$m, a silicon lens $t = 5000\,\mu$m and an antireflection coating on the lens surface for a frequency of 650 GHz ($\varepsilon = 3.4$, $t = 34\,\mu$m), to diminish the reflected wave from the lens/vacuum interface. The characteristic impedance of the resonator and the electromagnetic coupling element (coupler) was set to $Z_0 = 71\,\Omega$, which corresponds to a central conductor width of $10\,\mu$m centered relative to the gap of $50\,\mu$m and significantly reduces the effect of slot asymmetry in the areas of line turns within the resonator. The resonator allows the detector absorber to be matched with the external circuit $50\,\Omega$ for a certain (optimal) value of the nonlinear resistance $R(T_0)$. The coupling strength (level of split power) of the resonator with the excitation/readout line is determined by the length of the coupler section and the width of the shielding section between the central conductors. In the case of an RFTES

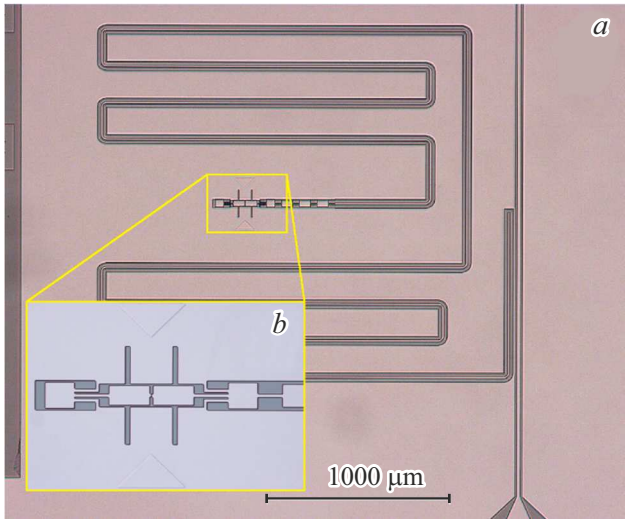

Figure 4. Micrographs of the experimental RFTES detector chip *L*-type: *a* — general view of the chip with a resonator and a double-slot antenna; *b* — enlarged, antenna of a new design; micro bridge size 1 by $3\,\mu$m of hafnium is located in the center of the antenna in the gap between electrodes $1\,\mu$m.

detector matrix, the value of the selected resonator Q-factor Q sets the density of the pump comb spectrum in a given frequency band and determines the detector's performance (the optimal response time of the resonator should be less than or equal to the time of the electron-phonon interaction). For the experimental detector, the Q-factor of the resonator was $Q \sim 5 \cdot 10^4$, which corresponded to the coupler length of $800\,\mu$m and the width of the shielding section of $10\,\mu$m in the area of the line-resonator coupling section.

When designing the circuit, a resistive absorber emulator was used, integrated into a linearly polarized double-slot planar antenna. The *S*-parameters and input impedance Z_{in} for ports in the antenna band of 600–700 GHz were calculated; the carrier frequency was chosen as $\sim 1.5\,\text{GHz} \pm 50\,\text{kHz}$. It is known that such a planar antenna in combination with an immersion lens can operate in the diffraction limit and has a gain of about 30 dBi with side lobes at the level of $-18\,$dB [16]. A special feature of the antenna design is the built-in inductive shunt, which somewhat complicates its structure, as shown in Fig. 4.

The optimization of the antenna beam pattern (ABP) aims to its axial symmetry, which helps to reduce the level of losses to the side lobes, as well as reducing cross-polarization by varying the length of the slots l and the distance d between them. Antenna analysis, assuming a sinusoidal current distribution along the slots, gives expressions for l and d, which at the antenna's carrier frequency of 650 GHz are 130 and $72\,\mu$m, respectively [16]. The EM calculation of the double-slot antenna in the band of 600–700 GHz showed a good matching of the antenna and the bridge: reflection losses were about $-9\,$dB, the signal leakage from the antenna into the resonator through the band-stop filters was less $-30\,$dB. The antenna beam

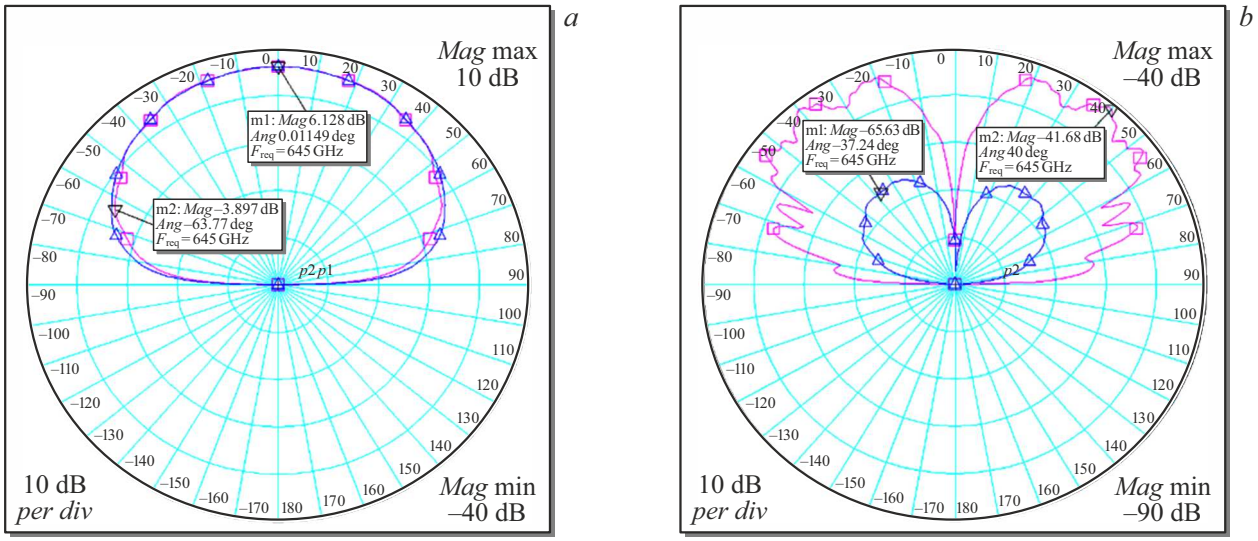

Figure 5. The bottom of the antenna shown in Fig. 4, at a frequency of 650 GHz. *a* — two main sections of the bottom, demonstrating good axial symmetry of the main lobe of reception; *b* — the level of cross-polarization, which characterizes the quality linear polarization of the antenna (preferably 40 dB).

pattern shown in Fig. 5 (the main lobe is directed into the substrate) has good axial symmetry and has a reception angle at the angle -10 dB of about 65°, which fits inside the angle of total internal reflection of the silicon lens, i.e., only a negligible part of the antenna reception diagram is cut off. The calculated cross-polarization level of the main sections is less than -40 dB. To match the bridge inside the antenna (Fig. 4, *b*) with the resonator, the insertion point corresponding to $|Z_{in}^{Res}| = |Z_{in}^{Ant}|$ was found. The geometry of the inductive shunts and the width of the antenna slots ($7.5\,\mu$m) were selected for a bridge with a resistance of $5\,\Omega$ (assuming $T_0 = 0.95 \cdot T_c$). The dip of $S_{21} = -6$ dB at the antenna feed point at the resonator frequency is predicted. Thus, the simulation of the complete electrodynamic system confirms the possibility of implementing both a L detector and an effective differential circuit in the resistance range of the bridge $3 - 6\,\Omega$.

The samples were fabricated in a clean area of NUST MISIS. A maskless Heidelberg μPG 501 laser lithograph with a resolution of about $1\,\mu$m was used to form the topology of the microstructure on a high-resistance silicon substrate. A thin film of hafnium with a thickness of about 30 nm was applied by magnetron sputtering at a residual pressure of $8 \cdot 10^{-8}$ mbar, argon sputtering pressure of $5 \cdot 10^{-3}$ mbar. The bridges are formed using lift-off lithography process. The resistance of the hafnium film at room temperature was $70\,\Omega/\square$; the critical temperature of the film T_c was about 200 mK. Before deposition of the niobium film (~ 100 nm), *in-situ* argon plasma cleaning was performed to remove impurities from the surface of the hafnium film. The deposition rate for niobium is 33 nm/min and 50 nm/min for hafnium. The niobium resonator and reading line are formed by plasma chemical etching in a mixture of gases CF_4/O_2 through a photoresist mask. Fig. 4 shows micrographs of the experimental chip. It should be noted that the presence of Andreev mirrors in the RFTES detector at the bridge/niobium electrode interface, according to the authors, is not a necessary condition for the trapping of hot electrons in the bridge volume, since the presence of natural hafnium film oxide with a thickness of about 5 nm (according to XRR analysis) is a barrier to the escape of hot electrons, but it does not prevent microwave heating of the electronic subsystem. A direct experiment comparing the thermal insulation of an absorber with a passivated hafnium layer and with Andreev mirrors is planned over the next year.

The transmission coefficient of the circuit S_{21} was measured in this experiment depending on the power of the pump signal; Agilent Technologies N5242A vector network analyzer was used. The chip was mounted in a holder with two SMP40 type coaxial connectors and connected to the measuring circuit by ultrasonic bonding onto the printed circuit board of the holder, which was installed in a Triton DR200 (Oxford Instruments) dilution refrigerator at the stage of mixing of ^{3}He/^{4}He. The experiment was conducted at a temperature of about 130 mK. A high-frequency signal of 1.5 GHz was supplied through attenuators with a total attenuation of 36 dB to suppress thermal noise of 300 K. Two buffer amplifiers were used with a total gain of 52 dB and a noise temperature reduced to the chip output of about 20K. The cooled amplifier was installed at stage 3 K and connected to the chip holder using a superconducting cable with low thermal conductivity; the second amplifier was installed outside the cryostat and provided amplification sufficient to suppress the intrinsic noise of the circuit meter. The resonator data obtained in the experiment corresponded with reasonable accuracy to the preliminary calculation. The deviation of the resonant

frequency from the calculated value of 1.5GHz was about 1%, Q-factor with zero bridge heating was 25 %, the value of the frequency offset when changing the nature of the impedance in the bridge circuit was 15 %. It should be noted that in the circuit with microwave supply lines there is no possibility of direct measurement of the resistance of the absorber bridges. A positive consequence of this situation is the almost complete absence of EMI (electro-magnetic intreference) at low frequencies, while the high-Q resonator also suppresses EMI at communication frequencies (mobile network, Bluetooth, WiFi).

As mentioned above, in addition to the inductive shunt, a parasitic bridge inductance occurs in the system, which leads to a change (shift) in the resonant frequency of the system when the bridge is in an unheated (superconducting) state. This new effect resembles the kinetic effect in MKID in our experiment. As can be seen from Fig. 6, there is a smooth shift in the resonant frequency with an increase of the pump frequency of 1.5 GHz. The kinetic effect found in Ref. [9] is manifested in an extended hafnium film, but in the case considered here, the bridge is short, the span effect is impossible, and hot electrons, especially those excited by a relatively low-frequency displacement current, are trapped in its volume. To summarize, in our case, the detector absorber cannot work effectively in the kinetic mode, and linear electromagnetic modeling predicts the behavior of the system accurately enough, shown in Fig. 6.

It should be noted the unusual behavior of the transmission coefficient in the form of small steps S_{21}, especially noticeable on the left slope of the resonance scanning area and more smoothed on the right. This behavior resembles an abrupt change in the bandwidth level in a coplanar transmission line, which includes *RF*-SQUID. In such a metamaterial junctions occur in Ref. [17] between stable states with different values of the magnetic susceptibility of the metamaterial, initiated by a change in the pumping power in the line. In our case, the presence of a superconducting loop in the antenna, closed by a bridge, probably leads to its abrupt switching from a superconducting state to a normal state and back to a superconducting one, which reflects the property of magnetic flux quantization in a doubly connected superconducting loop. This effect requires further study, for example, by analyzing the effect of an external magnetic field on the nature of the switching. Probably, it is possible to get rid of this effect by breaking the superconducting loop with a short bridge or an overhead contact made of normal metal.

An analysis of the data on the detector's response to heating by pumping current in minimum transmission $|S_{21}|^2$ is shown in Fig. 7; these dependencies are extracted from the data in Fig. 6. It should be noted that the derivative of the response has a variable sign compared to the previously measured *C*-type detector, which is consistent with the prediction of the numerical model of the *L*-detector (Fig. 1, *d*).

The area of low pumping levels is noteworthy, where efficiency reaches peak values, and the bolometer mode

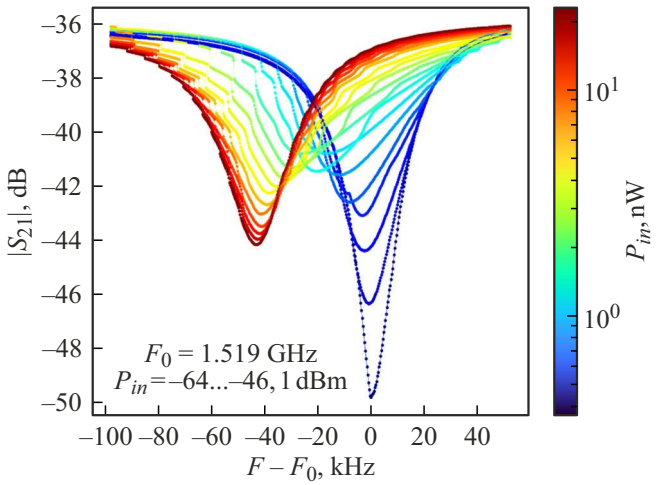

Figure 6. A family of dependencies of the transmittance $|S_{21}|^2$ of detector pumping line on the VNA pumping power on the chip.

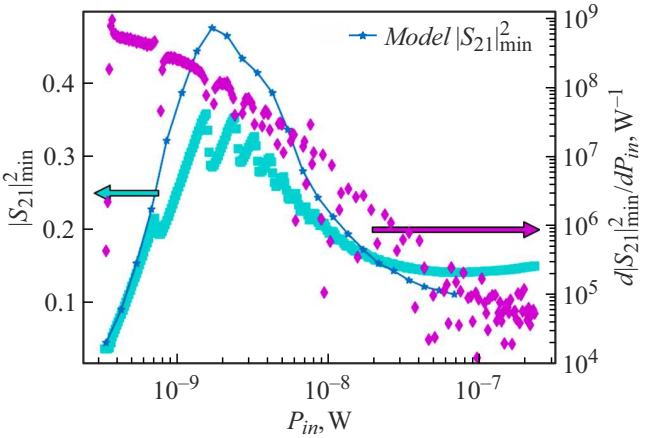

Figure 7. Dependence of the depth of the stop-band, $\min(|S_{21}|^2)$, and its derivative in heating power, $d(\min|S_{21}|^2)/dP_{in}$, — bolometer conversion efficiency.

remains stable (Fig. 7). It should be noted that the experimental dependence $|S_{21}|^2_{\min}$ confirms the simulation results quite well (a thin line, an analog of the dependence from Fig. 1, *d*).

The conversion coefficient (gain) of the detector is defined as [7]:

$$Gain = \frac{P_{in} d|S_{21}|^2}{|S_{31}|^2 dP_{in}} \quad (1)$$

The coefficient $|S_{31}|^2$ characterizes the transfer of heating power from the input port of the chip *1* to the port *3*, where the absorber is connected. The value of $|S_{31}|^2$ was found by adjusting the parameters of the lumped model circuit (Fig. 2, *b*) to the experimental data of the transmission coefficient $|S_{21}|$. The results of calculating the conversion coefficient for experimental and model transmission data are shown in Fig. 8. The model coefficient $|S_{31}|^2$, shown in

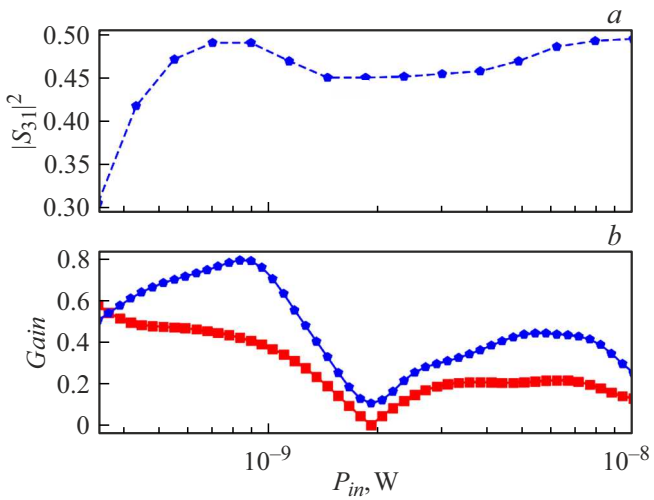

Figure 8. Dynamic characteristics of the detector: *a* — dependence of the coefficient of transfer of heating power from the input of the chip to the absorber, ($|S_{31}|^2$), calculated for the model circuit; *b* — gain on the bias power P_{in} for the experimental (red squares) and model curve (blue hexagons).

Fig. 8, *a*, and the data $\min(|S_{21}|^2)$ from Fig. 7 were used to calculate the gain coefficient for the two curves in Fig. 8, *b*.

Demonstration of alternating response was one of the main objectives of the experiment. At the same time, in the region of low heating (at the output of the absorber from the superconducting state), the response of the new detector has the same positive sign as the *C*-detector, but significantly steeper than the negative *L*-response observed at levels above −60 dBm, as shown by the data analysis shown in Fig. 7. The drop of *Q* at high pump levels (above −50 dBm) is probably attributable to an increase in losses in the niobium film (in the inductive shunt) due to an increase in microwave current density. It should be noted that the required current density in the resonator can be reduced by reducing the size of the bridge. Analysis of experimental data showed that when the RFTES detector absorber was heated with a carrier signal power at a frequency of 1.5 GHz, the following were obtained: the maximum of the amplitude response $d|S_{21}|^2/dP_{in} = 9 \cdot 10^8\ \mathrm{W}^{-1}$ and the maximum of the frequency (phase) response within an inductive transition $dF/dP_{in} = 3.2 \cdot 10^{13}$ Hz/W. Here, it is interesting to optimize the Q-factor of the detector in the region of a rapid shift of the resonant frequency with increasing heating (phase response), since such a response may be more effective than the amplitude response under certain conditions. It should be noted that, despite the fact that the observed response is similar to the kinetic one, it is the response of a thermoresistive element incorporated in a special way into the resonator. What is common with the kinetic effect in a superconductor here is the presence of two parallel conduction channels, an inductive and a resistive one, the ratio of which is controlled by a superconducting thermistor.

Conclusion

The results of the study confirm the main provisions of the new concept of an inductively coupled RFTES detector, as well as the methods used for calculating, designing and manufacturing experimental chips. Preliminary tests of the RFTES detector of *L*-type at a temperature of about 130 mK using heating of the bridges with microwave carrier showed good agreement with the calculated transmission parameters of S_{21}, responsible for carrier modulation with a terahertz signal. The effect of the resonance frequency shift upon the bridge's transit from the superconducting (low-impedance) state, which was previously estimated as a parasitic phenomenon, was evaluated. Apparently, the study of this effect is of particular interest when using a *L*-type detector in the phase response mode. As a continuation of this study, it is planned to test a new detector with a blackbody radiator source in the terahertz range, evaluate its optical NEP and conversion efficiency using a proven technique described in Ref. [2], including the detector test as part of a practical differential detector.

Funding

The study was supported by a grant from the Russian Science Foundation 24-29-20298 „Active Terahertz RFTES detector“ https://rscf.ru/project/24-29-20298 /.

Conflict of interest

The authors declare that they have no conflict of interest.

References

[1] S.V. Shitov. Tech. Phys. Lett., **37** (10), 932 (2011). DOI: 10.1134/S1063785011100117
[2] A.V. Merenkov, T.M. Kim, V.I. Chichkov, S.V. Kalinkin, S.V. Shitov. FTT, **64** (10), 1404 (2022). (in Russian) DOI: 10.21883/PSS.2022.10.54223.50HH
[3] S.V. Shitov, N.Yu. Rudenko, E.R. Khan. *Sverhprovodyashchij SVCh detektor prohodyashchej moshchnosti* (№2025102663: zayavl. 07.02.2025)
[4] S.V. Shitov. *Kamera distancionnogo temperaturnogo kontrolya* (Patent RU 188 418 U1 Rossijskaya Federaciya, MPK G01N 21/00 (2006.01, №2018146576: zayavl. 26.12.2018: opubl. 11.04.2019)
[5] S.V. Shitov. *Aktivnyj sverhprovodyashchij detektor* (Patent RU 2 801 961 C1 Rossijskaya Federaciya, MPK H01L 23/00 (2006.01), №2022134753: zayavl. 28.12.2022: opubl. 18.08.2023)
[6] A. Kuzmin, S.V. Shitov, A. Scheuring, J.M. Meckbach, K.S. Il'in, S. Wuensch, A.V. Ustinov, M. Siegel. IEEE Trans. Terahertz Sci. Tech., **3** (1), 25 (2013). DOI: 10.1109/TTHZ.2012.2236148
[7] A.V. Merenkov V.I. Chichkov, A.V. Ustinov, S.V. Shitov. J. Phys.: Conf. Ser., **1182**, 012009 (2019). DOI: 10.1088/1742-6596/1182/1/012009

[8] L.S. Solomatov, S.V. Shitov. Sb. statej po materialam XIX Mezhdunar. simp. Nanofizika i nanoelektronika, **1**, 91 (2025) (in Russian).
[9] S.V. Shitov, T.M. Kim, L.S. Solomatov, N.Yu. Rudenko, A.V. Merenkov, A.B. Ermakov, V.I. Chichkov. ZhTF, **94** (7), 1060 (2024) (in Russian). DOI: 10.61011/JTF.2024.07.58341.168-24
[10] S.V. Shitov. ZhTF, **93** (7), 988 (2023) (in Russian). DOI: 10.21883/JTF.2023.07.55758.116-23
[11] S.V. Shitov. *Differencial'nyj sverhprovodyashchij detektor* (Patent RU 2 801 920 C1 Rossijskaya Federaciya, MPK H01L 23/00 (2006.01), №2022134754: zayavl. 28.12.2022: opubl. 18.08.2023) (in Russian).
[12] P.K. Day, H.G. LeDuc, B.A. Mazin, A. Vayonakis, J. Zmuidzinas. Nature, **425**, 817 (2003). DOI: 10.1038/nature02037
[13] A.V. Uvarov, S.V. Shitov, A.N. Vystavkin. Uspekhi sovremennoy radioelectroniki, **8**, 43 (2010).
[14] N.Y. Rudenko, S.V. Shitov. ZhTF, **94** (11), 1828 (2024) (in Russian).
[15] Electronic source. Available at: Cadence AWR Microwave Office https://www.awr.com/awr-software/products/awr-design-environment
[16] D.F. Filipovic, S.S. Gearhart, G.M. Rebeiz. IEEE Trans. Microw. Th. Tech., **41** (10), 1738 (1993). DOI: 10.1109/22.247919
[17] P. Jung, S. Butz, M. Marthaler, M.V. Fistul, J. Leppäkangas, V.P. Koshelets, A.V. Ustinov. Nat. Commun., **5**, 3730 (2014). DOI: 10.1038/ncomms4730

Translated by A.Akhtyamov

Translated by A.Akhtyamov